6

The Linear Endfire Array Antenna

In this chapter we will treat the special situation where the main beam of a linear array antenna is directed alongside the array axis instead of perpendicular to this axis. The latter situation - treated in the previous two chapters - is known as broadside radiation, the first one we designate, for obvious reasons, *endfire* radiation. For an endfire array antenna, the radiating elements need to exhibit a radiation pattern that allows radiation into the endfire direction. Dipole radiators show a radiation pattern in the plane perpendicular to the dipole axis that satisfies this requirement. Therefore, the endfire specifics will be demonstrated in this chapter employing dipole radiators. To show that mutual coupling between radiators in array antenna - briefly mentioned in the previous chapter - is not necessarily an unwanted phenomenon, we will provide an approximate analysis of a Yagi–Uda array antenna in detail. A Yagi–Uda array antenna is a linear endfire array antenna consisting of dipole radiators, where only one element is driven and the other ones are excited by a mutual coupling mechanism.

6.1 INTRODUCTION

In the chapter on linear broadside array antennas we have seen that, for sufficiently small inter-element distances, a broadside beam is generated, provided that the array feeding network is not introducing phase shifts between the elements. We have also seen that if the inter-element distance is equal to or exceeds one wavelength, the array forms additional beams (grating lobes) at or near endfire.

The phase shifts introduced by the inter-element distances determine the number of beams, while additional phase shifts introduced by the feeding network or otherwise have the effect of dispositioning the main beam from its broadside direction. In this chapter we will look at the specific phase differences needed for creating endfire

Array and Phased Array Antenna Basics Hubregt J. Visser
 ISBN: 0-470-87117-2

operation. The general subject of beam scanning will be treated in the next chapter on linear *phased* array antennas.

In the previous chapters we have employed the concept of *pattern multiplication*. The array antenna radiation pattern was obtained by multiplying the array factor with the element factor or element radiation pattern. The element radiation pattern was seen to have a filtering effect on the array factor. For the aperture elements considered thus far, the radiation pattern is cosine-like, being at maximum in broadside direction and at minimum in endfire direction. Obviously, such a radiating element will not allow an endfire operation of the linear array antenna. We have also seen that a dipole radiator has a radiation pattern that is rotationally symmetric around the dipole axis and at maximum for directions perpendicular to the dipole axis centre. Therefore, we will demonstrate endfire radiation of a linear array antenna by employing dipole elements.

To create endfire operation of a linear array antenna we need to establish a phase difference between the elements for fixed inter-element distances. These phase differences may be introduced by the linear array feeding network. Either a corporate or parallel feeding network or a series feeding network will introduce mechanical difficulties (e.g. the need for different layers, see for example [1]) and the feeding network may take part in, or even disturb the radiation.

We may considerably simplify the array antenna architecture by only feeding one dipole, having the other (short-circuited) dipole elements in the linear array acting as parasites. The desired inter-element phase shifts are accomplished then by virtue of mutual coupling. For (thin) dipole radiators, the mutual coupling can be calculated with a practical level of accuracy with relative ease,[1] thus enabling the analysis of a Yagi–Uda endfire array antenna.

Before we start with the analysis of the Yagi–Uda array antenna, we will first have to establish the theoretical description of a linear endfire array antenna, for the moment not bothering about feeding networks or how to accomplish additional phase shifts between radiating elements. Then we need to talk about mutual coupling in general and finally describe the mutual interaction between two dipoles of different lengths.

6.2 PHASE DIFFERENCES

We start with considering a linear array antenna consisting of K elements, equally interspaced a distance d. The direction of a wave is described by the angle ϑ between rays and array normal, see figure 6.1.

We describe the array antenna in the receive situation.

The array factor, $S_a(\vartheta)$, for this linear array antenna is given by

$$S_a(\vartheta) = \sum_{i=1}^{K} e^{j(K-i)kd\sin(\vartheta)}, \tag{6.1}$$

where $k = \frac{2\pi}{\lambda}$ is the wave number with λ being the wavelength.

[1] In general, for arrays of thick or non-dipole radiators, this is not true.

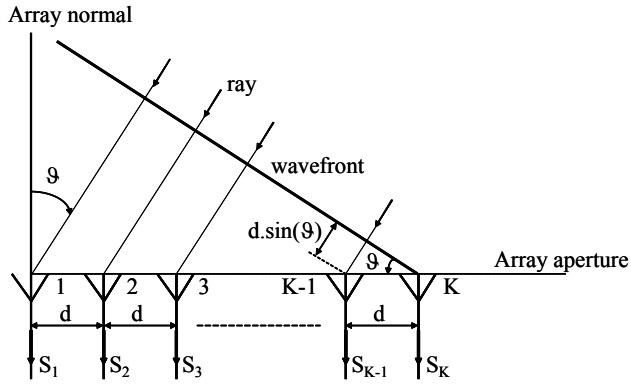

Fig. 6.1 Linear array of K elements.

If we now allow a linear phase taper to be existent over the array, meaning that every element of the array antenna adds a progressive phase α, the radiation pattern of the array antenna, $S(\vartheta)$, becomes

$$S(\vartheta) = f(\vartheta) \sum_{i=1}^{K} a_i e^{j(K-i)kd\sin(\vartheta)}, \tag{6.2}$$

where

$$a_i = e^{j(K-i)\alpha}, \tag{6.3}$$

and $f(\vartheta)$ is the element pattern.

The linear array radiation pattern may be written as

$$S(\vartheta) = f(\vartheta) \sum_{i=1}^{K} e^{j(K-i)\psi}, \tag{6.4}$$

where

$$\psi = kd\sin(\vartheta) + \alpha. \tag{6.5}$$

The maximum of the radiation pattern is obtained for $\psi = 0$, so for endfire operation at $\vartheta = 90°$, the additional phase difference, α, between two adjacent elements should be

$$\alpha = -kd\sin(90°) = -kd. \tag{6.6}$$

For endfire operation at $\vartheta = -90°$, the phase difference should be

$$\alpha = -kd\sin(-90°) = kd. \tag{6.7}$$

As we have already discussed, grating lobes occur whenever the argument ψ is an integer multiple of 2π,

$$\psi = n2\pi,\ n \in \mathbf{N}. \tag{6.8}$$

So, when $\alpha = -kd$ (endfire operation at $\vartheta = 90°$), grating lobes occur for

$$\frac{d}{\lambda}\left[\sin(\vartheta) - 1\right] = n, \;\; n \in \mathbf{N}. \tag{6.9}$$

For $d = \lambda$, four solutions exist: $\vartheta = 0$ for $n = -1$, $\vartheta = 90°$ for $n = 0$, $\vartheta = 180°$ for $n = -1$ and $\vartheta = -90°$ for $n = -2$, corresponding to three additional (grating) lobes next to the main beam ($n = 0$). This is shown in figure 6.2 for a linear array of eight isotropic elements, placed one wavelength apart.

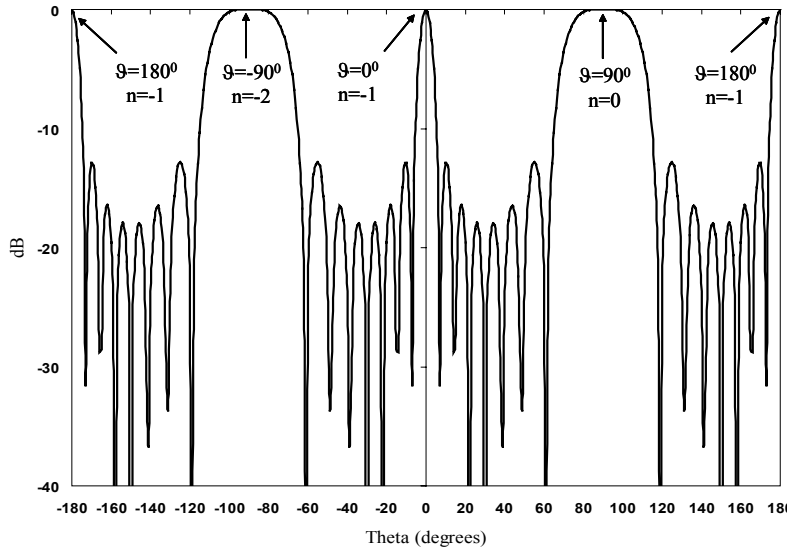

Fig. 6.2 Linear array of eight isotropic elements, placed one wavelength apart, phased for endfire operation at $\vartheta = 90°$, normalised to radiation maximum.

If we reduce the element spacing to a half wavelength, two solutions exist: $\vartheta = 90°$ for $n = 0$ and $\vartheta = -90°$ for $n = -1$, see figure 6.3 for a linear array of eight isotropic elements, placed half a wavelength apart.

So, for a broadside linear array antenna we could place the elements as far apart from each other as one wavelength, before grating lobes started to occur. For a endfire linear array antenna it appears that the maximum allowable element distance preventing the occurrence of grating lobes has reduced to half a wavelength. If we reduce the element spacing below half a wavelength, the grating lobe at $\vartheta = -90°$ in figure 6.3 will disappear.

The theoretical explanation of this phenomenon will be given in the next chapter where we will discuss beam scanning in a linear array antenna.

We will conclude the discussion on grating lobes in endfire array antennas, by showing that for a linear array, having an inter-element spacing smaller than half a wavelength, indeed only one endfire beam does exist. Figure 6.4 shows the normalised radiation pattern of a linear array consisting of eight isotropic elements, spaced four-tenths of a wavelength apart.

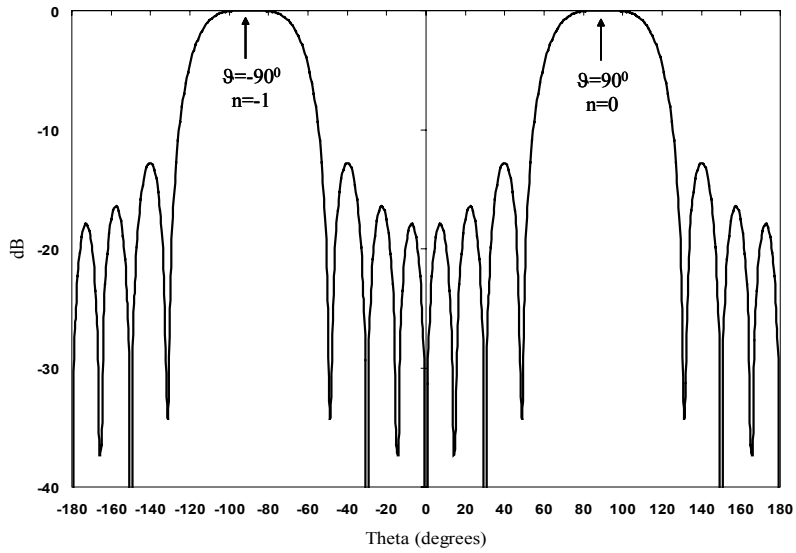

Fig. 6.3 Linear array of eight isotropic elements, placed half a wavelength apart, phased for endfire operation at $\vartheta = 90°$, normalised to radiation maximum.

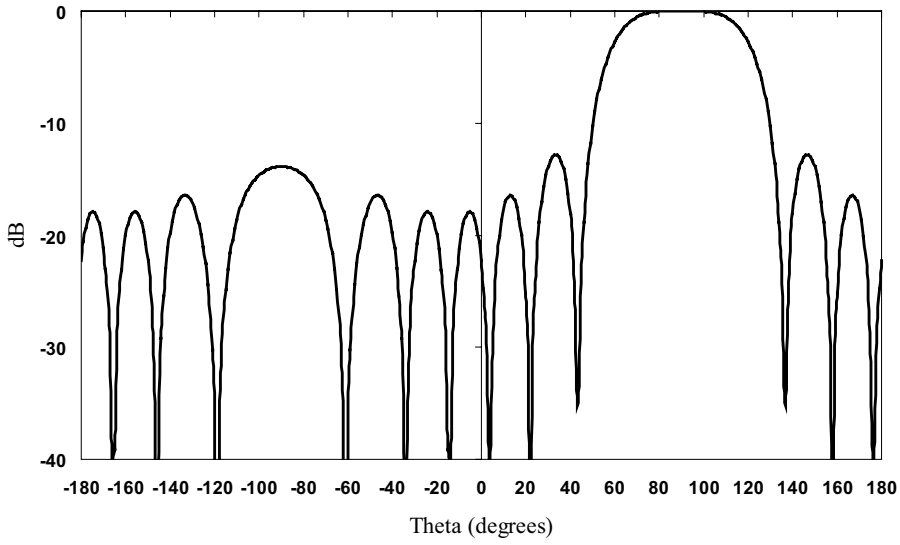

Fig. 6.4 Linear array of eight isotropic elements, placed four-tenths of a wavelength apart, phased for endfire operation at $\vartheta = 90°$, normalised to radiation maximum.

In fact, by choosing an element distance smaller than half a wavelength, we have moved the maximum of the grating lobe out of the *visible* into the *invisible region.*[2]

[2]The visible region is defined by angles ϑ for which $|\sin(\vartheta)| \leq 1$. In this situation, that corresponds to angles $-180° \leq \vartheta \leq 180°$.

The *back lobe* we see in figure 6.4 is formed by the part of the grating lobe still present in the visible region.

If we want the back lobe to be removed altogether, the argument, ψ, for endfire operation at $\vartheta = 90°$ should, at $\vartheta = -90°$ be equal to $-\pi$,

$$\psi|_{\vartheta=-90°} = kd\,[\sin(\vartheta) - 1]|_{\vartheta=-90°} = -\pi, \tag{6.10}$$

so

$$d = \frac{\lambda}{4}, \tag{6.11}$$

where use has been made of $k = \frac{2\pi}{\lambda}$.

Figure 6.5 shows the normalised radiation pattern for an eight-element linear array of isotropic radiators, spaced a quarter of a wavelength apart and phased for $\vartheta = 90°$ endfire operation.

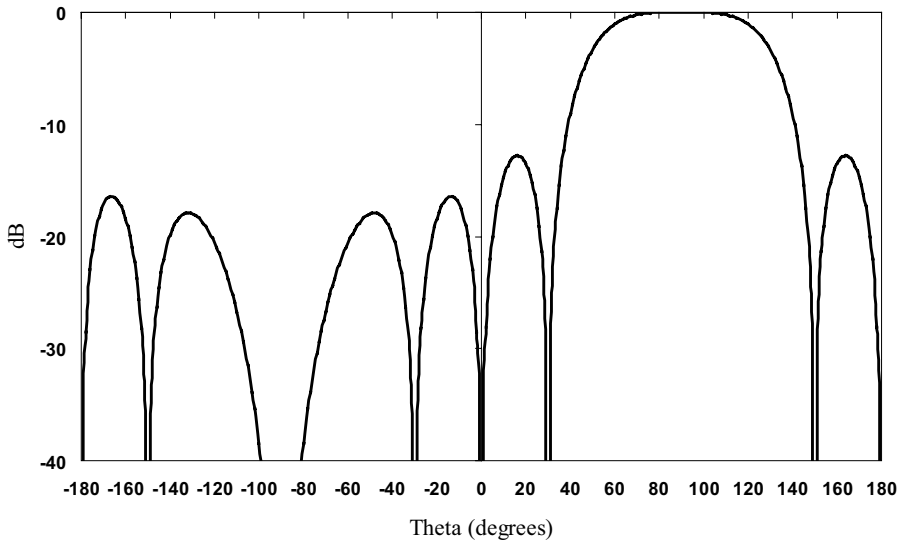

Fig. 6.5 Linear array of eight isotropic elements, placed a quarter of a wavelength apart, phased for endfire operation at $\vartheta = 90°$, normalised to radiation maximum.

The figure shows that for this element distance, the grating lobe effects - normally visible in a backfire lobe - have indeed completely disappeared.

For the linear endfire array antennas treated thus far, the linear phase taper over the array elements ($\alpha = \mp kd$) compensates exactly the phase delay of waves in the desired endfire direction. These endfire arrays are called *ordinary endfire arrays*. This naming implies also that 'extraordinary' endfire arrays must exist. In the next section we will briefly discuss the *Hansen–Woodyard endfire array*.

6.3 HANSEN–WOODYARD ENDFIRE ARRAY ANTENNA

For long array antennas (i.e. much longer than one wavelength) of closely spaced elements, a higher directivity (smaller main beam) may be obtained than for the ordinary endfire array antenna. This may be accomplished by having an additional phase difference, α', applied to adjacent array elements that is slightly larger than the phase delay a wave experiences travelling in the endfire direction

$$\alpha' = \mp(kd + \delta). \tag{6.12}$$

The minus sign applies for a radiation maximum at $\vartheta = 90°$ and the plus sign applies for a radiation maximum at $\vartheta = -90°$.

In 1938, Hansen and Woodyard [2] proposed for δ in the above equation [3, 4]

$$\delta = \frac{2.94}{K-1} \approx \frac{2.94}{K} \approx \frac{\pi}{K}. \tag{6.13}$$

The linear array antenna radiation pattern may be written then as

$$S(\vartheta) = f(\vartheta) \sum_{i=1}^{K} e^{j(K-i)\psi'}, \tag{6.14}$$

where

$$\psi' = kd\sin(\vartheta) \mp \left(kd + \frac{\pi}{K}\right), \tag{6.15}$$

in which the minus sign applies for endfire operation at $\vartheta = 90°$ and the plus sign applies for endfire operation at $\vartheta = -90°$.

Figure 6.6 shows the normalised radiation patterns of a linear array of eight isotropic radiators, phased for ordinary and for Hansen–Woodyard endfire operation at $\vartheta = 90°$ for an element spacing of half a wavelength.

We do see a smaller beam in the desired endfire direction, but at the same time we observe back lobe levels that are in excess of the main beam level. Obviously, the additional phase difference, δ, has yielded a sharper main lobe, but this additional phase shift has also caused the rise of the back lobes. The only way to decrease the back lobe level to values less than that of the main beam lies in decreasing the element spacing and thus accomplishes bringing the argument ψ' closer to $-\pi$ for $\vartheta = -90°$ [4, 5].[3]

To demonstrate this, in figure 6.7 the normalised radiation patterns are shown of a linear array of eight isotropic radiators, phased for ordinary and for Hansen–Woodyard endfire operation at $\vartheta = 90°$ for an element spacing of four-tenths of a wavelength.

We do indeed observe a lowering of the back lobe level.

If we want to achieve a maximum suppression of the back lobe - for the array antenna phased for Hansen–Woodyard endfire operation at $\vartheta = 90°$ - the following

[3]For the linear array antenna operated at $-90°$ endfire, the argument ψ' should be brought closer to $+\pi$ for $\vartheta = 90°$.

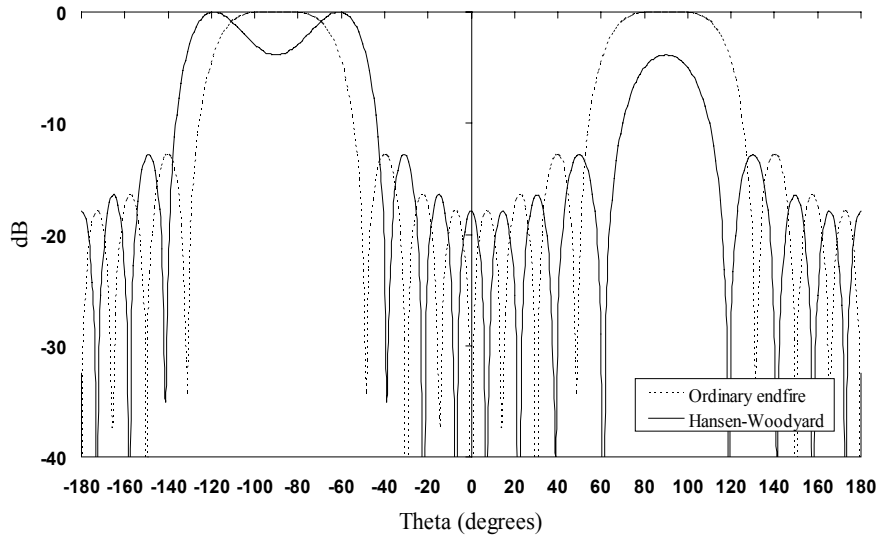

Fig. 6.6 Linear array of eight isotropic elements, placed half a wavelength apart, phased for ordinary and for Hansen–Woodyard endfire operation at $\vartheta = 90°$, normalised to radiation maximum.

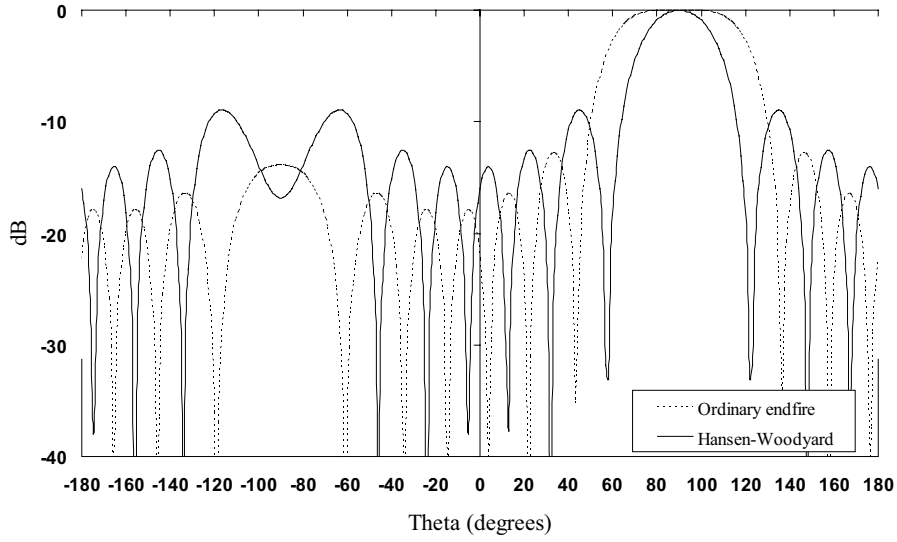

Fig. 6.7 Linear array of eight isotropic elements, placed four-tenths of a wavelength apart, phased for ordinary and for Hansen–Woodyard endfire operation at $\vartheta = 90°$, normalised to radiation maximum.

condition should apply

$$\psi'|_{\vartheta=-90^\circ} = \left[kd\sin(\vartheta) - \left(kd + \frac{\pi}{K}\right)\right]\Big|_{\vartheta=-90^\circ} = -\pi, \tag{6.16}$$

which leads to

$$d = \frac{K-1}{K}\frac{\lambda}{4} \approx \frac{\lambda}{4}. \tag{6.17}$$

Figure 6.8 shows the normalised radiation patterns of a linear array of eight isotropic radiators, phased for ordinary and for Hansen–Woodyard endfire operation at $\vartheta = 90^\circ$ for an element spacing of a quarter of a wavelength.

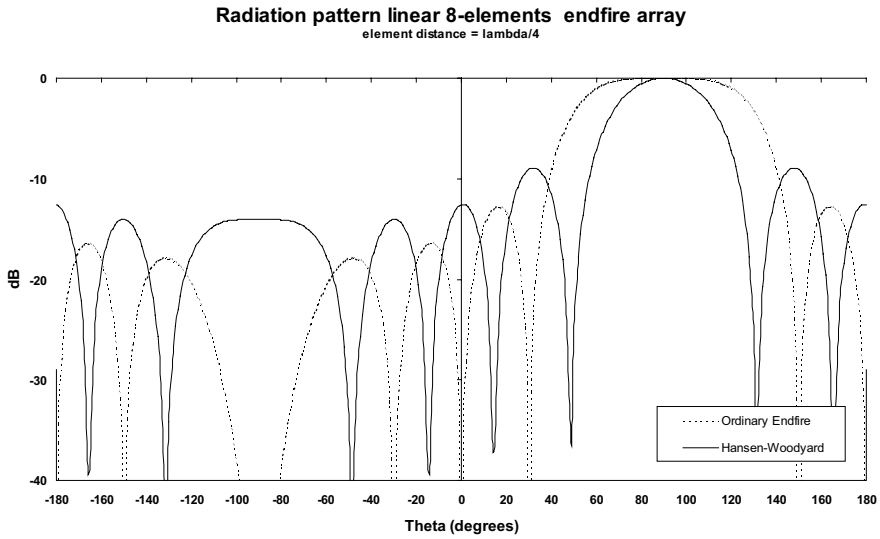

Fig. 6.8 Linear array of eight isotropic elements, placed a quarter of a wavelength apart, phased for ordinary and for Hansen–Woodyard endfire operation at $\vartheta = 90^\circ$, normalised to radiation maximum.

So, by satisfying the Hansen–Woodyard criterion ($\alpha = \mp\left(kd + \frac{\pi}{K}\right)$) in a linear endfire array antenna, a higher directivity (smaller main beam) may be accomplished. But since there is no such thing as a free lunch, the price to be paid is an increased side lobe and back lobe level, as figure 6.8 clearly demonstrates.

6.4 MUTUAL COUPLING

At the beginning of this chapter we said that we were intending to accomplish the desired phase shift between the linear endfire array antenna elements by virtue of *mutual coupling*. To that end we will first discuss mutual coupling between array antenna elements in general terms, before we go into the details of designing an endfire dipole array antenna.

Consider two antenna elements, 1 and 2 [5]. A voltage generator, V_1, is attached to antenna-element 1 that acts as transmitting element, while the current I_2, is measured at the terminals of antenna-element 2, that acts as receiving element. The set-up is shown in figure 6.9a. If we apply a voltage generator V_2 to antenna-element 2, we will measure a current I_1 at the terminals of antenna-element 1, see figure 6.9b.

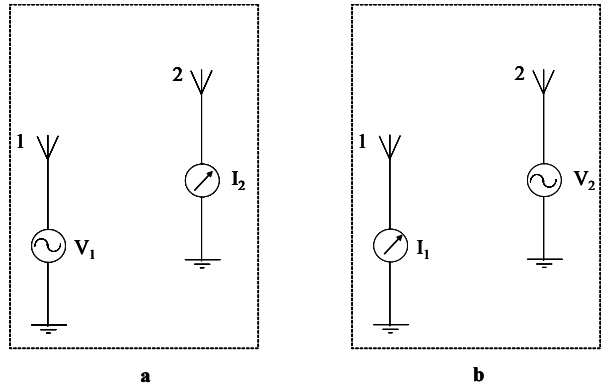

Fig. 6.9 Two-element array antenna set-up. a. Antenna-element 1 is transmitting, antenna-element 2 is receiving. b. Antenna-element 2 is transmitting, antenna-element 1 is receiving.

The ratio of voltage to current is an impedance. For the situation depicted in figure 6.9a, we call the ratio of voltage V_1 to current I_2 a *transfer impedance* or *mutual impedance*:

$$\frac{V_1}{I_2} = Z_{12}. \tag{6.18}$$

Similarly, for the situation depicted in figure 6.9b:

$$\frac{V_2}{I_1} = Z_{21}, \tag{6.19}$$

and by virtue of antenna reciprocity[4]

$$Z_{21} = Z_{12}. \tag{6.20}$$

If we now consider the situation where we only have antenna 1 present, excited by voltage generator V_1 and we measure the current I_1 at its terminals, we may define the input impedance as

$$Z_{11} = \frac{V_1}{I_1}. \tag{6.21}$$

Bringing antenna 2 in the neighbourhood of antenna 1, will mean that - through radiation[5] - a current I_2 is induced on this antenna by antenna 1. This current I_2 will

[4]If $V_1 = V_2$ in figure 6.9, then $I_2 = I_1$.
[5]Next to direct space radiation, mutual coupling may also occur through scattering from nearby objects and by reflections through and radiation from the array antenna feed network.

cause radiation from antenna 2 and thus will influence the current on antenna 1. This phenomenon is called *mutual coupling*.

The total voltage at antenna 1 may then be written as

$$V_1 = Z_{11}I_1 + Z_{12}I_2, \tag{6.22}$$

where Z_{11} and Z_{12} are as defined before

$$Z_{11} = \left.\frac{V_1}{I_1}\right|_{I_2=0}, \tag{6.23}$$

and

$$Z_{12} = \left.\frac{V_1}{I_2}\right|_{I_1=0}. \tag{6.24}$$

Similarly

$$V_2 = Z_{21}I_1 + Z_{22}I_2, \tag{6.25}$$

where

$$Z_{21} = \left.\frac{V_2}{I_1}\right|_{I_2=0}, \tag{6.26}$$

$$Z_{22} = \left.\frac{V_2}{I_2}\right|_{I_1=0}. \tag{6.27}$$

This discussion of a two-element array antenna may be generalised to a K-element array antenna for which

$$\begin{aligned} V_1 &= Z_{11}I_1 + Z_{12}I_2 + \cdots + Z_{1K}I_K \\ V_2 &= Z_{21}I_1 + Z_{22}I_2 + \cdots + Z_{2K}I_K \\ &\vdots \\ V_K &= Z_{K1}I_1 + Z_{K2}I_2 + \cdots + Z_{KK}I_K \end{aligned}, \tag{6.28}$$

where

$$Z_{mn} = \left.\frac{V_m}{I_n}\right|_{I_i=0, i\neq n}. \tag{6.29}$$

The input impedance, Z_m, of the m^{th} element in the array, including all mutual coupling - also known as the *active impedance* - is then

$$Z_m = \frac{V_m}{I_m} = Z_{m1}\frac{I_1}{I_m} + Z_{m2}\frac{I_2}{I_m} + \cdots + Z_{mm} + \cdots + Z_{mK}\frac{I_K}{I_m}. \tag{6.30}$$

Since current is the origin of electromagnetic radiation, the mutual coupling will not only affect the input impedances of the elements in the array, but also their radiation patterns. The mutual coupling effects will in general change with element position, angle of radiation and frequency and will depend on the type of array element under consideration. Thus, in general, the calculation of mutual coupling

effects will be difficult.[6] However, for some practical situations, approximations may be made that make an analytical treatment of coupling effects feasible. One such a practical situation occurs for arrays of thin dipole radiators, e.g. Yagi–Uda endfire array antennas.

6.5 YAGI–UDA ARRAY ANTENNA

The Yagi–Uda array antenna consists of a number of dipole elements, of which only one is driven. The other dipole elements act as parasitic radiators, the radiation stemming from currents induced by mutual coupling. The array is an endfire array. Usually there is one element next to the driver at one side and multiple elements next to the driver at the other side. The one element is generally longer than the driver and acts as reflector, the elements on the other side of the driver usually are shorter than the driver and act as directors, see figure 6.10.

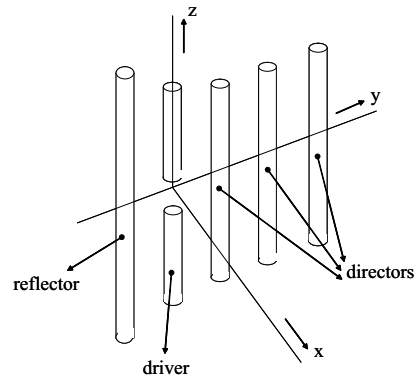

Fig. 6.10 Five-element Yagi–Uda array antenna, one reflector, three directors. The endfire operation is in the x, y-plane in the y-direction. The elements have an omnidirectional radiation pattern in the x, y-plane.

The origin of this type of array antenna stems from Japan at the end of the 1920s and was first published about by S. Uda. The first English written publication on this array antenna was by H. Yagi, a co-worker of Uda [4] and for long the antenna has been known as the Yagi-antenna. Recently the antenna has been called the *Yagi–Uda Array Antenna* to give credit to both inventors.

[6]In the chapter on array antenna measurement we will treat the concept of the *active* or *scan element pattern*, i.e. the radiation pattern of one driven element in its array environment where all other elements are terminated into matched loads. For large array antennas, an average active element pattern may be factored out of the array antenna radiation pattern, making a pattern multiplication between active element pattern and array factor without mutual coupling possible. All mutual coupling effects are accounted for then in the average active element pattern.

6.5.1 Mutual Impedance

To calculate the mutual impedances between the elements in a Yagi–Uda array antenna, we need to be able to calculate the mutual impedance between two, nonstaggered (meaning that the imaginary line through the centres of the dipoles is perpendicular to both dipoles), unequal length dipole elements as shown in figure 6.11.

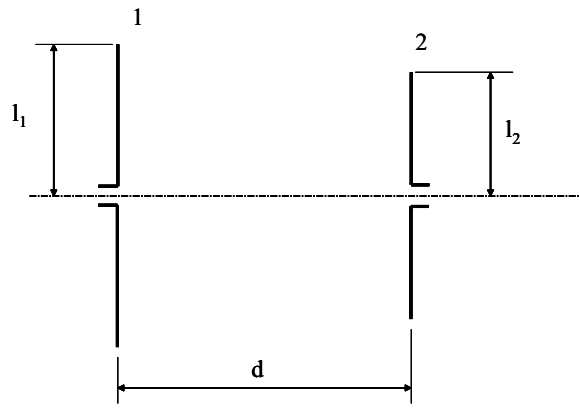

Fig. 6.11 Two, unstaggered, unequal length dipole elements.

In this figure, d is the distance between the two dipole elements and l_1 and l_2 are the half-lengths of, respectively, dipole 1 and dipole 2.

Analytical expressions for the mutual impedance, Z_{12}, for this situation are derived by King [6], employing the *induced emf* method (for an explanation of the induced emf method, see, for example [4]). The results are obtained under the assumption of infinitely thin dipoles supporting sinusoidal currents, and are shown to be valid for wire radii at least up to $10^{-5}\lambda$ [4]. λ is the used wavelength.

The currents on both dipole elements are

$$I_i = I_{i0} \begin{cases} \sin\left[k\left(z_i + l_i\right)\right] & \text{for } -l_i \leq z_i \leq 0 \\ \sin\left[k\left(l_i - z_i\right)\right] & \text{for } 0 \leq z_i \leq l_i \end{cases} \tag{6.31}$$

for $i = 1, 2$, where z_i is the local coordinate along the dipole i and l_i is the half-length of dipole i. I_{i0} is the amplitude of the current on dipole i, and k is the wave number, $k = \frac{2\pi}{\lambda}$.

The mutual impedance is then found to be [6]

$$Z_{12} = R_{12} + jX_{12}, \tag{6.32}$$

where

$$\begin{aligned} R_{12} = 30 \{ & \cos[k(l_1+l_2)] \cdot \\ & [C_i(u_0) + C_i(v_0) - C_i(u_1) - C_i(v_1) - C_i(w_1) - C_i(y_1) + 2C_i(kd)] + \\ & \cos[k(l_1-l_2)] \cdot \\ & [C_i(u_0') + C_i(v_0') - C_i(u_1) - C_i(v_1) - C_i(w_1) - C_i(y_1) + 2C_i(kd)] + \\ & \sin[k(l_1+l_2)] \cdot [-S_i(u_0) + S_i(v_0) + S_i(u_1) - S_i(v_1) - S_i(w_1) + S_i(y_1)] + \\ & \sin[k(l_1-l_2)] \cdot [-S_i(u_0') + S_i(v_0') + S_i(u_1) - S_i(v_1) + S_i(w_1) - S_i(y_1)] \}, \end{aligned} \tag{6.33}$$

and

$$\begin{aligned} X_{12} = 30 \{ & \cos[k(l_1+l_2)] \cdot \\ & [-S_i(u_0) - S_i(v_0) + S_i(u_1) + S_i(v_1) + S_i(w_1) + S_i(y_1) - 2S_i(kd)] + \\ & \cos[k(l_1-l_2)] \cdot \\ & [-S_i(u_0') - S_i(v_0') + Si(u_1) + S_i(v_1) + S_i(w_1) + S_i(y_1) - 2S_i(kd)] + \\ & \sin[k(l_1+l_2)] \cdot [-C_i(u_0) + C_i(v_0) + C_i(u_1) - C_i(v_1) - C_i(w_1) + C_i(y_1)] + \\ & \sin[k(l_1-l_2)] \cdot [-C_i(u_0') + C_i(v_0') + C_i(u_1) - C_i(v_1) + C_i(w_1) - C_i(y_1)] \}. \end{aligned} \tag{6.34}$$

In the above equations

$$u_0 = k\left[\sqrt{d^2 + (l_1+l_2)^2} - (l_1+l_2)\right], \tag{6.35}$$

$$v_0 = k\left[\sqrt{d^2 + (l_1+l_2)^2} + (l_1+l_2)\right], \tag{6.36}$$

$$u_0' = k\left[\sqrt{d^2 + (l_1-l_2)^2} - (l_1-l_2)\right], \tag{6.37}$$

$$v_0' = k\left[\sqrt{d^2 + (l_1-l_2)^2} + (l_1-l_2)\right], \tag{6.38}$$

$$u_1 = k\left[\sqrt{d^2 + l_1^2} - l_1\right], \tag{6.39}$$

$$v_1 = k\left[\sqrt{d^2 + l_1^2} + l_1\right], \tag{6.40}$$

$$w_1 = k\left[\sqrt{d^2 + l_2^2} + l_2\right], \tag{6.41}$$

$$y_1 = k\left[\sqrt{d^2 + l_2^2} - l_2\right]. \tag{6.42}$$

The *sine integral* $S_i(x)$ is defined as

$$S_i(x) = \int_0^x \frac{\sin(\rho)}{\rho} d\rho, \tag{6.43}$$

and the *cosine integral* is defined as

$$C_i(x) = -\int_x^\infty \frac{\cos(\rho)}{\rho} d\rho = \int_\infty^x \frac{\cos(\rho)}{\rho} d\rho. \tag{6.44}$$

Sine and cosine integrals are well tabulated, see for example [7], and subroutines are readily available for most programming languages, [8].

The real and imaginary part of the *self-impedance* of element i, R_i and X_i respectively, are taken from [1] for dipole lengths $2l_i$ and wire radii a satisfying $1.3 \leq kl \leq 1.7$ and $0.0016 \leq \frac{a}{\lambda} \leq 0.01$.

$$R_i = \sum_{m=0}^{4} \sum_{n=0}^{4} a_{mn} (kl_i)^m \left(\frac{a}{\lambda}\right)^{-n}, \tag{6.45}$$

$$X_i = \sum_{m=0}^{4} \sum_{n=0}^{4} b_{mn} (kl_i)^m \left(\frac{a}{\lambda}\right)^{-n}, \tag{6.46}$$

where, [1][7]

$$\begin{pmatrix} a_{00} & a_{01} & a_{02} & a_{03} & a_{04} \\ a_{10} & a_{11} & a_{12} & a_{13} & a_{14} \\ a_{20} & a_{21} & a_{22} & a_{23} & a_{24} \\ a_{30} & a_{31} & a_{32} & a_{33} & a_{34} \\ a_{40} & a_{41} & a_{42} & a_{43} & a_{44} \end{pmatrix} =$$

$$\begin{pmatrix} 0.484315 \cdot 10^4 & -0.475502 \cdot 10^2 & 0.237406 \\ -0.137680 \cdot 10^5 & 0.134736 \cdot 10^3 & -0.671429 \\ 0.147939 \cdot 10^5 & -0.144272 \cdot 10^3 & 0.717576 \\ -0.716807 \cdot 10^4 & 0.699523 \cdot 10^2 & -0.346901 \\ 0.134304 \cdot 10^4 & -0.130631 \cdot 10^2 & 0.644693 \cdot 10^{-1} \end{pmatrix}$$

$$\begin{pmatrix} -0.517831 \cdot 10^{-3} & 0.387725 \cdot 10^{-6} \\ 0.146303 \cdot 10^{-2} & -0.109502 \cdot 10^{-5} \\ -0.156154 \cdot 10^{-2} & 0.116801 \cdot 10^{-5} \\ 0.753029 \cdot 10^{-3} & -0.562448 \cdot 10^{-6} \\ -0.139347 \cdot 10^{-3} & 0.103804 \cdot 10^{-6} \end{pmatrix}, \tag{6.47}$$

[7]The '-n' powers in equations (6.45) and (6.46) have been introduced by the author to make these equations work with the coefficients as stated in Elliot's book [1] and as reproduced in equations (6.47) and (6.48). The original equations in [1] have '+n' powers, but for the correct equations the coefficients are erroneous. The correct coefficients are tabulated in the revised version of Elliot's book [12]. The altered equations with the original coefficients give results comparable to those obtained with the correct equations and correct coefficients.

and

$$\begin{pmatrix} b_{00} & b_{01} & b_{02} & b_{03} & b_{04} \\ b_{10} & b_{11} & b_{12} & b_{13} & b_{14} \\ b_{20} & b_{21} & b_{22} & b_{23} & b_{24} \\ b_{30} & b_{31} & b_{32} & b_{33} & b_{34} \\ b_{40} & b_{41} & b_{42} & b_{43} & b_{44} \end{pmatrix} =$$

$$\begin{pmatrix} -0.644754 \cdot 10^4 & 0.767385 \cdot 10^2 & -0.360563 \\ 0.189983 \cdot 10^5 & -0.237542 \cdot 10^3 & 0.110722 \cdot 10^1 \\ -0.209803 \cdot 10^5 & 0.267034 \cdot 10^3 & -0.124666 \cdot 10^1 \\ 0.102804 \cdot 10^5 & -0.131818 \cdot 10^3 & 0.619050 \\ -0.188863 \cdot 10^4 & 0.245077 \cdot 10^2 & -0.115922 \end{pmatrix}$$

$$\begin{pmatrix} 0.709234 \cdot 10^{-3} & -0.488904 \cdot 10^{-6} \\ -0.218661 \cdot 10^{-2} & 0.151517 \cdot 10^{-5} \\ 0.247753 \cdot 10^{-2} & -0.172674 \cdot 10^{-5} \\ -0.123956 \cdot 10^{-2} & 0.869298 \cdot 10^{-6} \\ 0.233996 \cdot 10^{-3} & -0.165155 \cdot 10^{-6} \end{pmatrix}. \tag{6.48}$$

We now assume a Yagi–Uda linear endfire array antenna consisting of K elements. The driven element is designated number 1, the reflector is number 2[8] and the $K-2$ directors are numbered in increasing order, moving away from the driven element, see figure 6.12.

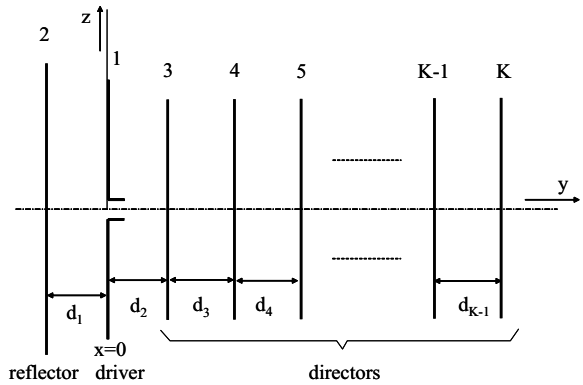

Fig. 6.12 Element designation for a K element Yagi–Uda linear endfire array antenna.

As shown in figure 6.12, all dipole elements, except for the driven one, are short-circuited. Therefore, the antenna may be described using equation (6.28), with all

[8]The reflector element is longer than the driven element, the directors in general are shorter. Because of the thus created reflective properties of the second element, adding additional reflector elements in general does not alter the antenna characteristics and in practice more than two reflecting elements are hardly ever encountered. In our analysis we restrict ourselves to having just one reflector element.

voltages, except V_1, equal to zero

$$\begin{aligned}
V_1 &= Z_{11}I_1 + Z_{12}I_2 + \cdots + Z_{1i}I_i + \cdots + Z_{1,K-1}I_{K-1} + Z_{1K}I_K \\
0 &= Z_{21}I_1 + Z_{22}I_2 + \cdots + Z_{2i}I_i + \cdots + Z_{2,K-1}I_{K-1} + Z_{2K}I_K \\
&\vdots \\
0 &= Z_{i1}I_1 + Z_{i2}I_2 + \cdots + Z_{ii}I_i + \cdots + Z_{i,K-1}I_{K-1} + Z_{iK}I_K \\
&\vdots \\
0 &= Z_{K1}I_1 + Z_{K2}I_2 + \cdots + Z_{Ki}I_i + \cdots + Z_{K,K-1}I_{K-1} + Z_{KK}I_K.
\end{aligned} \tag{6.49}$$

The last $K-1$ equations may be rewritten into

$$\begin{pmatrix} -Z_{21} \\ -Z_{31} \\ \vdots \\ -Z_{i1} \\ \vdots \\ -Z_{K-1,1} \\ -Z_{K1} \end{pmatrix} = \begin{pmatrix} Z_{22} & Z_{23} & \cdots & Z_{2i} & \cdots & Z_{2K} \\ Z_{32} & Z_{33} & \cdots & Z_{3i} & \cdots & Z_{3K} \\ \vdots & \vdots & \vdots & \vdots & \vdots & \vdots \\ Z_{i2} & Z_{i3} & \cdots & Z_{ii} & \cdots & Z_{iK} \\ \vdots & \vdots & \vdots & \vdots & \vdots & \vdots \\ Z_{K-1,2} & Z_{K-1,3} & \cdots & Z_{K-1,i} & \cdots & Z_{K-1,K} \\ Z_{K2} & Z_{K3} & \cdots & Z_{Ki} & \cdots & Z_{KK} \end{pmatrix} \begin{pmatrix} \dfrac{I_2}{I_1} \\ \dfrac{I_3}{I_1} \\ \vdots \\ \dfrac{I_i}{I_1} \\ \vdots \\ \dfrac{I_{K-1}}{I_1} \\ \dfrac{I_K}{I_1} \end{pmatrix}. \tag{6.50}$$

The system can be solved for the unknown current ratios by taking the inverse of the impedance matrix

$$[I] = [Z]^{-1}[V], \tag{6.51}$$

where

$$[I] = \left[\frac{I_2}{I_1}, \frac{I_3}{I_1}, \ldots, \frac{I_K}{I_1}\right]^T, \tag{6.52}$$

$$[V] = [-Z_{21}, -Z_{31}, \ldots, -Z_{K1}]^T, \tag{6.53}$$

and

$$[Z] = \begin{bmatrix} Z_{22} & Z_{23} & \cdots & Z_{2i} & \cdots & Z_{2K} \\ Z_{32} & Z_{33} & \cdots & Z_{3i} & \cdots & Z_{3K} \\ \vdots & \vdots & \vdots & \vdots & \vdots & \vdots \\ Z_{i2} & Z_{i3} & \cdots & Z_{ii} & \cdots & Z_{iK} \\ \vdots & \vdots & \vdots & \vdots & \vdots & \vdots \\ Z_{K-1,2} & Z_{K-1,3} & \cdots & Z_{K-1,i} & \cdots & Z_{K-1,K} \\ Z_{K2} & Z_{K3} & \cdots & Z_{Ki} & \cdots & Z_{KK} \end{bmatrix}, \tag{6.54}$$

where $^{-1}$ means taking he inverse and ^{T} means taking the transpose.

Once the system has been solved for the unknown induced currents, $I_2, I_3, \ldots, I_K$, in terms of the current I_1, the input impedance, Z_{in}, of the Yagi–Uda antenna may be calculated as

$$Z_{in} = \frac{V_1}{I_1} = Z_{11} + Z_{12}\frac{I_2}{I_1} + Z_{13}\frac{I_3}{I_1} + \cdots + Z_{1i}\frac{I_i}{I_1} + \cdots + Z_{1,K-1}\frac{I_{K-1}}{I_1} + Z_{1K}\frac{I_K}{I_1}. \quad (6.55)$$

When the impressed and induced currents are known, the radiated fields can be computed. I_1 is the impressed current, $I_2, I_3, \ldots, I_K$ are the induced currents.

6.5.2 Radiation

The far field of one finite length dipole element only has $\mathbf{E}_\vartheta$ and $\mathbf{H}_\varphi$ components[9] and - since the Maxwell equations that relate electric and magnetic fields are linear - the same applies to a Yagi–Uda antenna, see figure 6.13.

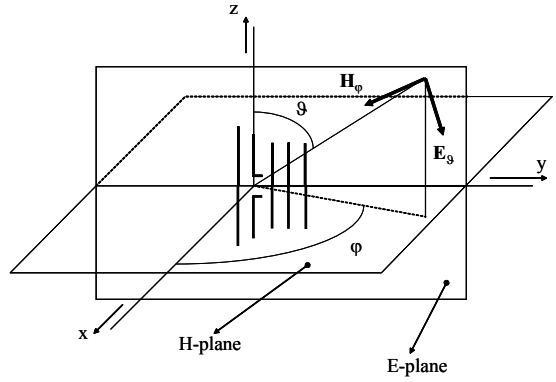

Fig. 6.13 Yagi–Uda antenna orientation.

The electric field component generated by dipole element i, E_{ϑ_i}, is calculated as [4]

$$E_{\vartheta_i} = -j\omega A_{\vartheta_i}, \quad (6.56)$$

where

$$A_{\vartheta_i} = -\frac{\mu_0 e^{-jkr}}{4\pi r}\sin(\vartheta)\int_{-l_i}^{l_i} I_i e^{jk(x_i\sin(\vartheta)\cos(\varphi)+y_i\sin(\vartheta)\sin(\varphi)+z_i\cos(\vartheta))}dz_i = -\frac{\mu_0 e^{-jkr}}{4\pi r}\sin(\vartheta)e^{jk(x_i\sin(\vartheta)\cos(\varphi)+y_i\sin(\vartheta)\sin(\varphi))}\int_{-l_i}^{l_i} I_i e^{jkz_i\cos(\vartheta)}dz_i. \quad (6.57)$$

Herein, l_i is the half-length of element i.

With the current distribution I_i as stated in equation (6.31) and for the situation as depicted in figures 6.12 and 6.13 ($x_i = 0\ \forall i$) the electric field component is calculated

[9]These components are perpendicular to one another and are interrelated through $H_\varphi = \frac{E_\vartheta}{\eta}$, where $E_\vartheta = |\mathbf{E}_\vartheta|$, $H_\varphi = |\mathbf{H}_\varphi|$ and $\eta = \sqrt{\frac{\mu_0}{\varepsilon_0}} \approx 120\pi\Omega$ and is called the *free space characteristic impedance.*

as

$$E_{\vartheta_i} = j60I_{i0}\frac{e^{-jkr}}{r}e^{jky_i\sin(\vartheta)\sin(\varphi)}\frac{\cos\left[kl_i\cos(\vartheta)\right]-\cos\left[kl_i\right]}{\sin(\vartheta)}, \tag{6.58}$$

where use has been made of

$$\frac{2\omega\mu_0}{4\pi k} = \frac{\eta}{2\pi} \approx \frac{120\pi}{2\pi} = 60. \tag{6.59}$$

The electric field component for the complete K-element Yagi–Uda array antenna may then be written as

$$E_\vartheta = j\frac{60}{\sin(\vartheta)}\frac{e^{-jkr}}{r}\sum_{i=1}^{K} I_{i0}e^{jky_i\sin(\vartheta)\sin(\varphi)}\left(\cos\left[kl_i\cos(\vartheta)\right]-\cos\left[kl_i\right]\right). \tag{6.60}$$

The antenna will be analysed in the E-plane and H-plane.

The E-plane is the plane containing the electric field vector and the direction of maximum radiation. In figure 6.13, the E-plane is the yz-plane ($\varphi = 90°$). The H-plane is the plane containing the magnetic field vector and the direction of maximum radiation. In figure 6.13, the H-plane is the xy-plane ($\vartheta = 90°$).

The electric fields in the E-plane and H-plane are given by, respectively

E-plane:

$$E_\vartheta = j\frac{60}{\sin(\vartheta)}\frac{e^{-jkr}}{r}\sum_{i=1}^{K} I_{i0}e^{jky_i\sin(\vartheta)}\left(\cos\left[kl_i\cos(\vartheta)\right]-\cos\left[kl_i\right]\right), \tag{6.61}$$

H-plane:

$$E_\vartheta = j60\frac{e^{-jkr}}{r}\sum_{i=1}^{K} I_{i0}e^{jky_i\sin(\varphi)}\left(1-\cos\left[kl_i\right]\right). \tag{6.62}$$

The field radiation pattern is proportional to $|rE_\vartheta|$. The normalised (field) radiation pattern $F(\vartheta)$ is given by

$$F(\vartheta) = \frac{|rE_\vartheta|}{|rE_{\vartheta_{max}}|}, \tag{6.63}$$

where $E_{\vartheta_{max}}$ is obtained from substitution of $\vartheta = 90°$ in equation (6.61) or substitution of $\varphi = 90°$ in equation (6.62).

$$E_{\vartheta_{max}} = j60\frac{e^{-jkr}}{r}\sum_{i=1}^{K} I_{i0}e^{jky_i}\left(1-\cos\left[kl_i\right]\right). \tag{6.64}$$

6.5.3 Antenna Design

The main advantage of the analysis described in the preceding paragraphs lies in its simplicity, allowing for the creation of a computer program that can analyse a multitude of configurations in a short time and thus optimise designs given some user-defined constraints.

To understand this, we will try a straightforward approach in the design of a Yagi–Uda array antenna, using the theory developed.

We will look at the most basic configuration, that consists of a driven dipole element and a single parasitic dipole element, longer than the driven element, that will act as reflector, see figure 6.14.

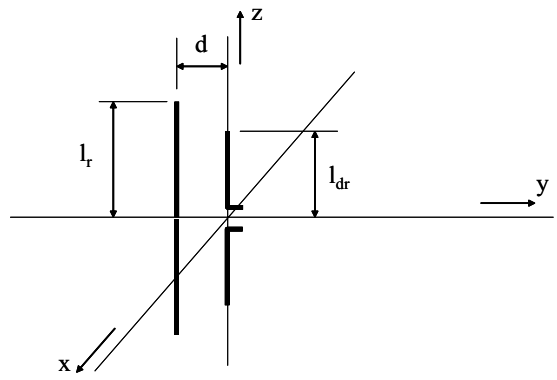

Fig. 6.14 Basic two-element Yagi–Uda array antenna configuration.

We choose the length of the driven dipole to be $2l_{dr} = 0.475\lambda$ and the length of the reflector $2l_r = 0.500\lambda$ and try to find the element distance d that ensures endfire operation along the positive y-axis.

We know that to ensure endfire operation in the desired direction, the phasing of the elements should be such that a phase difference $\alpha = -kd$ exists, see equations (6.5) and (6.6). For element distances, d, ranging between 0.025λ and 0.50λ, we have used the theory of the preceding paragraphs to calculate the phase of $\frac{I_2}{I_1}$, where I_1 is the excitation current of the driven element and I_2 is the induced current in the reflector. The results are shown in figure 6.15. In the same figure also $-kd$ as function of element distance d is shown.

We see that nowhere in the element distance range do we find a phasing that applies to the 90° endfire condition (see also [1]).

As a next try we do not pose the constraint of endfire operation at 90°, but we pose the constraint of a minimum at −90°, thus ensuring endfire operation at +90° [1]. Equations (6.5) and (6.6) learn that the phase of $\frac{I_2}{I_1}$ needs to be equal then to $-\pi+kd$. The curve of $-\pi + kd$ versus d is also shown in figure 6.15. Again there is no crossing with the phase curve of $\frac{I_2}{I_1}$.

As a last try, we look at the possibility to create endfire operation at −90°. To this end the phase of $\frac{I_2}{I_1}$ should be equal to $+kd$. In figure 6.15 we see that the phase curve of $\frac{I_2}{I_1}$ crosses the kd-curve at $d \approx 0.3\lambda$.

As a verification of the thus found element spacing, the H-plane radiation patterns of the two-element Yagi–Uda antenna are shown for different element spacings in figure 6.16.

The figure shows that the found element spacing $d \approx 0.30\lambda$ does *not* lead to an 'optimum' endfire result in the desired direction! The figure reveals an optimum

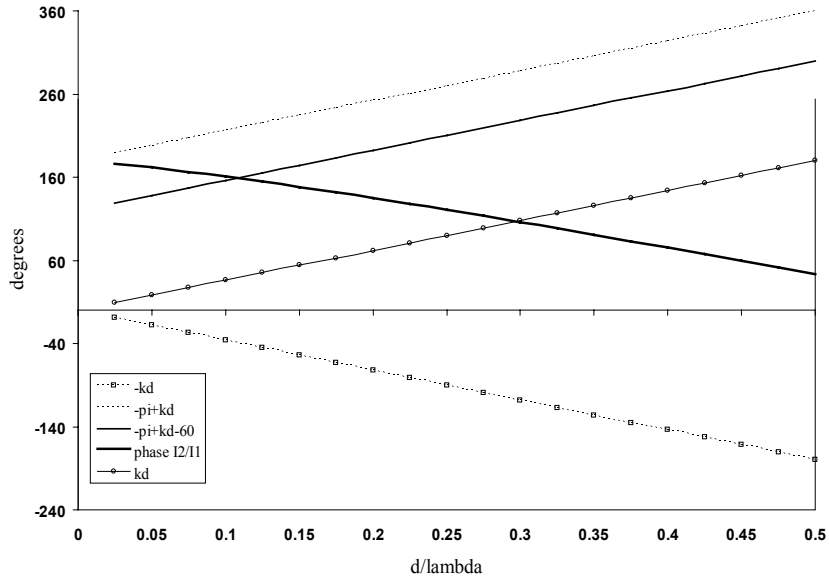

Fig. 6.15 Element phasing for the basic two-element Yagi–Uda array antenna configuration.

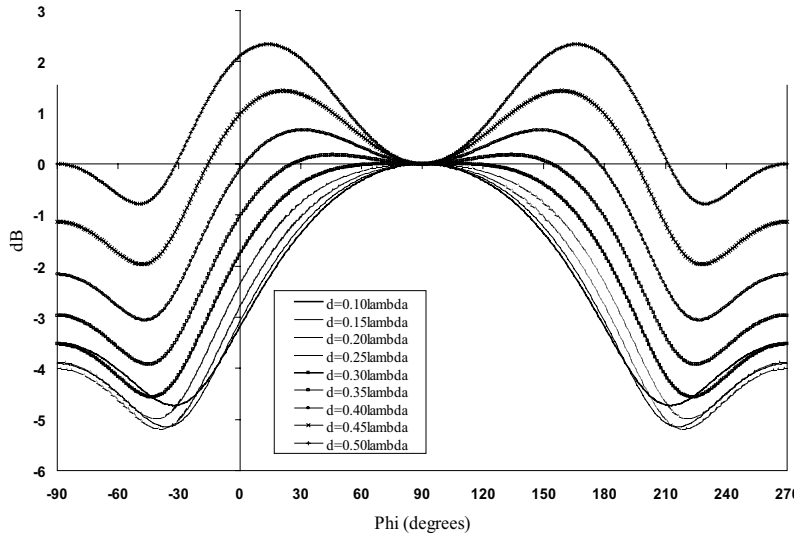

Fig. 6.16 H-plane radiation patterns for the basic two-element Yagi–Uda array antenna for different element spacings.

element distance $d \approx 0.15\lambda$. We also see that if the element distance increases, the phasing between the elements changes in such a way that the endfire operation changes into broadside operation.

The explanation lies in the fact that a Yagi–Uda array antenna is a travelling-wave antenna that supports a surface wave into the direction of endfire that has a phase velocity below that of the free space velocity of light [3, 9]. This means that the phase delay between the elements is greater than kd and that therefore the additional phase difference α between the elements should also be greater than kd. As figures 6.15 and 6.16 show, an additional phase shift of 60° leads - for this particular situation - to the desired element spacing.

As suggested in [1], the best way to find the optimum element spacing is to compute the antenna directivity as function of element spacing. The same applies to finding the optimum driver and reflector length. For Yagi–Uda antennas consisting of more than three elements, some sort of computer optimisation will certainly facilitate the design process. The theory as described before offers the advantage of simplicity, resulting in fast calculation times.

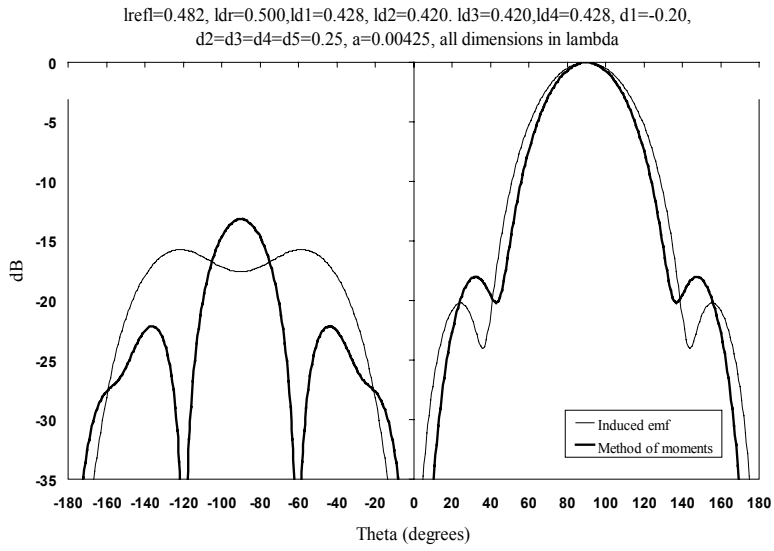

Fig. 6.17 E-plane power patterns for a six-element Yagi–Uda array antenna analysed by induced-emf method and method of moments.

This simplicity can also be a drawback, especially in the design of larger Yagi–Uda antennas. The assumption of sinusoidal currents on the array dipole elements is too crude and will lead to gross inaccuracies in the radiation pattern away from the main beam, especially in the back lobe region. It should be noted therefore that the theory was developed as an educational tool and care should be taken in employing this theory in a real Yagi–Uda antenna design tool. To that purpose, a point-matching

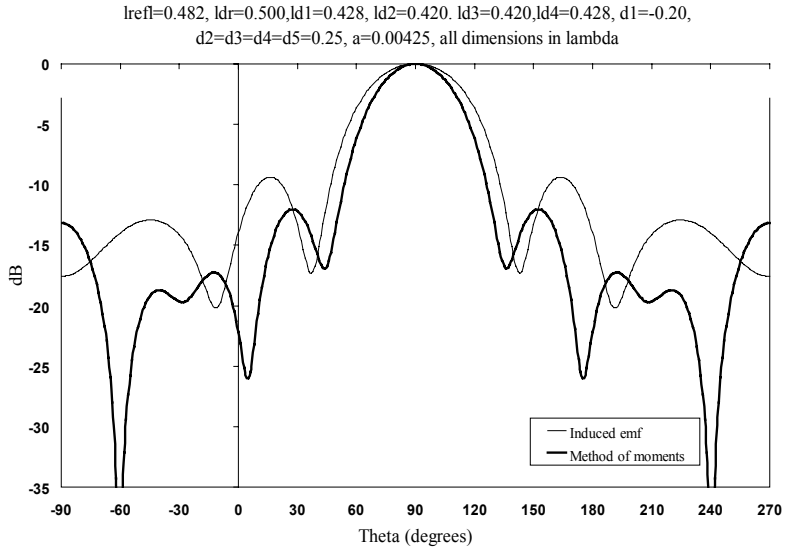

Fig. 6.18 H-plane power patterns for a six-element Yagi–Uda array antenna analysed by induced-emf method and method of moments.

version of the method of moments for the analysis of Yagi–Uda antennas [10] that is added as a Fortran routine to [4] may be employed.

As a demonstration, a six-element Yagi–Uda antenna is analysed, both by the induced-emf method and the method of moments. The results for the E-plane power pattern and the H-plane power pattern are shown in, respectively, figures 6.17 and 6.18. The dimensions of the antenna are taken from [11].

The fact that the E-plane radiation patterns seem to be more alike than the H-plane radiation patterns is due to the element-filtering characteristics in the E-plane. In the H-plane the element pattern is a constant.

REFERENCES

1. Robert S. Elliot, *Antenna Theory and Design*, Prentice-Hall, Englewood Cliffs, New Jersey, 1981.

2. W.W. Hansen and J.R. Woodyard, A New Principle in Directional Antenna Design, *Proceedings IRE*, Vol. 26, March 1938, pp. 333–345.

3. Warren L. Stutzman and Gary A. Thiele, *Antenna Theory and Design, second edition*, John Wiley & Sons, New York, 1998.

4. Constantine A. Balanis, *Antenna Theory and Design, second edition*, John Wiley & Sons, New York, 1997.

5. John D. Kraus, *Antennas*, McGraw-Hill, New York, 1950.

6. Howard E. King, Mutual Impedance of Unequal Length Antennas in Echelon, *IRE Transactions on Antennas and Propagation*, July 1957, pp. 306–313.

7. Milton Abramowitz and Irene A. Stegun (eds.), *Handbook of Mathematical Functions*, National Bureau of Standards Applied Mat., Government Printing Office, 1964.

8. W.H. Press, S.A. Teukolsky, W.T. Vetterling and B.P. Flanery, *Numerical Recipes, The Art of Scientific Computing*, Cambridge University Press, 1986.

9. H.W. Ehrenspeck and H. Poehler, A New Method for Obtaining Maximum Gain from Yagi Antennas, *IRE Transactions on Antennas and Propagation*, October 1959, pp. 379–386.

10. Gary A. Thiele, Analysis of Yagi–Uda Type Antennas, *IEEE Transactions on Antennas and Propagation*, Vol. AP-17, No. 1, January 1969, pp. 24–31.

11. Peter P. Viezbicke, Yagi Antenna Design, *National Bureau of Standard Technical Note 688*, December 1976.

12. Robert S. Elliot, *Antenna Theory and Design, revised edition*, John Wiley & Sons, New York, 2003.